ADVANCED THERAPEUTICS
www.advtherap.com

Near Infrared Photo-Antimicrobial Targeting Therapy for *Candida albicans*

*Hirotoshi Yasui, Kazuomi Takahashi, Shunichi Taki, Misae Shimizu, Chiaki Koike, Koji Umeda, Shofiqur Rahman, Tomohiro Akashi, Van Sa Nguyen, Yoshiyuki Nakagawa, and Kazuhide Sato**

Drug-resistant microorganisms are a pressing issue, and innovative antimicrobial therapies are required; antibodies targeting antigens on pathogen surfaces have emerged as one such modality. IgY, abundant in chicken egg yolk, confers passive immunity, and is effective against various pathogens; however, its antimicrobial effects remain limited. Near-infrared photoimmunotherapy (NIR-PIT), originally developed as a cancer treatment, specifically kills cancer cells via a photosensitizing phthalocyanine dye (IRDye700Dx; IR700)-conjugated monoclonal antibody, and irradiating NIR light. IgY-photo-antimicrobial targeting therapy (IgY-PAT^2), exploiting NIR-PIT, is investigated to destroy only microorganisms. IR700 is conjugated with anti-*Candida albicans* IgY (CA-IgY) to generate CA-IgY-IR700, which specifically binds various *Candida* spp. (and not human skin cells). The antimicrobial effect of CA-IgY-PAT^2 is dependent on the NIR-light dose ($p < 0.0001$). CA-IgY-PAT^2 significantly reduces the area of ulcers in a mouse model of CA-infected cutaneous ulcers ($p < 0.0001$), indicating that CA-IgY-PAT^2 is a new promising therapeutic method for CA infection.

1. Introduction

In recent years, many resistant bacteria have emerged due to antibiotic abuse, and the development of antibiotics has also stagnated.[1,2] Therefore, new antibacterial treatments that are different from conventional antibiotics are required. These should be potentially effective against a wide variety of pathogens, have no adverse effects, and should not impose a selection pressure that leads to the development of resistance in bacteria. Accordingly, multidisciplinary techniques with medical bioengineering to address this situation should be attempted.

Chicken egg yolk immunoglobulin (IgY) antibodies are transferred from the serum to egg yolk to impart passive immunity.[3] In the egg yolk, they are contained and accumulate at a higher concentration than that in the serum, and can be adjusted relatively easily and in large quantities. The effects of these antibodies have been confirmed in vitro and in vivo against various pathogens such as bacteria (*Pseudomonas aeruginosa*, *Acinetobacter baumannii*, *Helicobacter pylori*, *Streptococcus mutans*, etc.), virus (*influenza virus*, *hantavirus*, etc.), fungi (*Candida albicans* (CA)), with no adverse effects, resistant bacteria, or toxic residues. IgY is less likely to cause adverse reactions due to antibody-dependent cellular cytotoxicity or complement activation because IgY does not activate the mammalian complement or bind mammalian Fc receptors.[4,5] IgY is expected as one of

H. Yasui, K. Takahashi, S. Taki, Dr. K. Sato
Respiratory Medicine
Nagoya University Graduate School of Medicine
65 Tsuumai-cho, Showa-ku, Nagoya, Aichi 466-8550, Japan
E-mail: k-sato@med.nagoya-u.ac.jp

M. Shimizu, C. Koike
Advanced Analytical and Diagnostic Imaging Center (AADIC)/Medical Engineering Unit (MEU), B3 Unit
Nagoya University Institute for Advanced Research
65 Tsuumai-cho, Showa-ku, Nagoya, Aichi 466-8550, Japan

Dr. K. Umeda, Dr. S. Rahman, Dr. V. S. Nguyen
EW Nutrition Japan
Immunology Research Institute in Gifu
839-7, Gifu-City Sano, Gifu 501-1101, Japan

Dr. T. Akashi, Dr. Y. Nakagawa
Division of OMICS Analysis
Nagoya University Graduate School of Medicine
65 Tsuumai-cho, Showa-ku, Nagoya, Aichi 466-8550, Japan

Dr. T. Akashi
Division of Systems Biology
Nagoya University Graduate School of Medicine
65 Tsuumai-cho, Showa-ku, Nagoya, Aichi 466-8550, Japan

Dr. K. Sato
CREST, JST
Honcho Kawaguchi
Saitama 332-0012, Japan

Dr. T. Akashi
S-YLC
Nagoya University Institute for Advanced Research
Furo-cho, Chikusa-ku, Nagoya, Aichi 464-8601, Japan

The ORCID identification number(s) for the author(s) of this article can be found under https://doi.org/10.1002/adtp.202000221

DOI: 10.1002/adtp.202000221

the immunotherapeutic drugs suitable for mass production, and therapeutic approaches to SARS-CoV-2 in the actual COVID-19 pandemic context. Although the beneficial effects of IgY in immunotherapeutic strategies to control infectious disease are well established, this technology has some limitations. The transient nature of the protection makes the continuous administration of antibodies at effective doses imperative, resulting in limited success.[6,7] One possible way to improve this is to make naked IgY "arming" with photoabsorber, resulting in light activation. Then, in response to light, armed IgY could exert additional effects on bacteria.

Near infrared photoimmunotherapy (NIR-PIT) is a novel molecular-targeted cancer therapy that is involves the conjugation of a monoclonal antibody (mAb) with a photoabsorbing phthalocyanine dye, IRDye700Dx (IR700), which is activated by near-infrared (NIR) light irradiation. The mAb-IR700 conjugate is directed against mAb-specific surface proteins enriched on cancer cell membranes. The activation of IR700 upon NIR irradiation results in the specific rupture of the cell to which the mAb-IR700 conjugate is bound, entirely sparing the unbound normal cells.[8–15] An international phase III clinical trial of recurrent head and neck squamous cell carcinoma is currently underway to test this (LUZERA-301: https://clinicaltrials.gov/ct2/show/NCT03769506).

Similarly, photodynamic therapy (PDT) is used for cancer treatment with a combination of dye and light.[16] Although this technology was discovered 100 years ago based on its ability to kill various microorganisms, its application to infectious diseases is still in the development stage.[17–19] Some clinical trials on the use of PDT with aminolaevulinic acid (ALA) for infectious diseases have been performed; however, they had limited success, as PDT has no targeting ability.[20–22]

To make light therapy for infectious disease clinically applicable, we considered photo-antimicrobial targeting therapy (PAT^2), a multidisciplinary therapy that targets microbes by exploiting NIR-PIT with IgY (**Figure 1**). The employment of IgY for PAT^2 enables the use of a large number of inexpensive antibodies and management of pathogens with a high growth rate, which requires a large amount of antibodies. It could also be used to treat other pathogens by changing the antigen. Here, to prove the concept of PAT^2, we developed a new treatment for intractable *Candida* infections. The therapeutic effect was examined by comparing the effects of IgY-PAT^2 and conventional ALA-PDT, and subsequent biological reactions were analyzed to examine additional therapeutic effects.

2. Results and Discussion

Since the number of target cells and the growth rate are different between microorganisms and tumor cells, it was necessary to adjust conditions in order to apply NIR-PIT, which is originally a cancer treatment, to IgY-PAT^2, which is an antimicrobial treatment. Conditions such as the concentration of IR700 conjugated anti-*C. albicans*-IgY (CA-IgY-IR700) and NIR irradiation intensity were examined, and the effect of IgY-PAT^2 was evaluated. In vivo, using a mouse model of infectious skin ulcer, the effect of PAT2 was evaluated not only by ulcer area but also by multiple methods of bacterial count and inflammatory cytokines.

2.1. Purification of CA-IgY and Light Source Device

CA-IgY was extracted from the egg yolk of chicken immunized with inactivated CA and, then purified by using the Thiophilic Adsorption column. The unbound (UB) and bound (B) fractions was collected for further analyses. The result of the water-soluble fractions obtained during IgY extraction were analyzed by SDS-PAGE. The specialized column device yielded fractions that corresponded to a protein with high purity that is thought to be the IgY (**Figure 2**A). It showed a thick band in SDS-PAGE, which apparently represented the chicken IgY. As the purification was carried out under none denaturing conditions, the thick bands represented both chains of IgY. (Figure 2B). The molecular weight patterns agreed with the expected molecular mass for the heavy and light chains, respectively. The sizes were 68 and 27 kDa of egg yolk antibody IgY according to the protein ladder. The bands at 35 kDa might be the C-terminal fragment of the egg yolk protein vitellogenin II precursor.[7]

The purified IgY samples showed the total IgY concentration of CA-IgY was 2.25 mg mL^{-1} (Figure 2B) as measured by sandwich ELISA, an indication that this concentrated fractionated CA-IgY may have a better immunological response to pathogens.

We assembled a high-power light emitting diode (LED) at the wavelength of 630 or 690 nm, as the light source. The actual light intensity was measured with a power meter before the experiments (Figure 2C). The 690 nm LED is set for PAT^2, 630 nm is for ALA-PDT, respectively.

2.2. Conjugation of the CA-IgY and IR700DX

Chemical conjugation of the IgY and the photoabsorber IR700 was performed. The integrity of the CA-IgY-IR700 conjugate was confirmed, as evidenced by the strong binding between CA-IgY and IR700; however, CA-IgY alone did not exhibit any detectable fluorescent signals based on SDS-PAGE (**Figure 3**A). The final concentration of IgY was 1.18 mg mL^{-1} based on protein staining, and the overall recovery rate of CA-IgY was almost 90%. The molar concentration ratio was evaluated as 1 molecule of IgY to 3.5 molecules of IR700. Next, we evaluated the photolysis of IR700 after NIR light irradiation. The CA-IgY-IR700 was irradiated with NIR light and electrophoresed by SDS-PAGE. The fluorescence band decreased depending on the amount of NIR light, and almost disappeared at 256 J cm^{-2}. From this result, we determined 256 J cm^{-2} NIR irradiation as the maximum NIR irradiation dose (Figure 3B).

2.3. In Vitro Characterization of the Specific Binding of CA-IgY-IR700 to CA

Candida spp. and A431 cells were reacted with CA-IgY-IR700 whose concentration determined in a prior experiment (200 μg mL^{-1}) (Figure S1, Supporting Information). Fluorescent signals obtained using CA-IgY-IR700 from CA (JCM 1542, IFO 579, IFO 1060, IFO 1385, and FC18), *C. tropicalis*, *C. guilliermondii*, and *C. krusei* were evaluated, and fluorescent signals from these *Candida* spp. were found to have similar intensities. However, the intensity of fluorescent signals did not increase

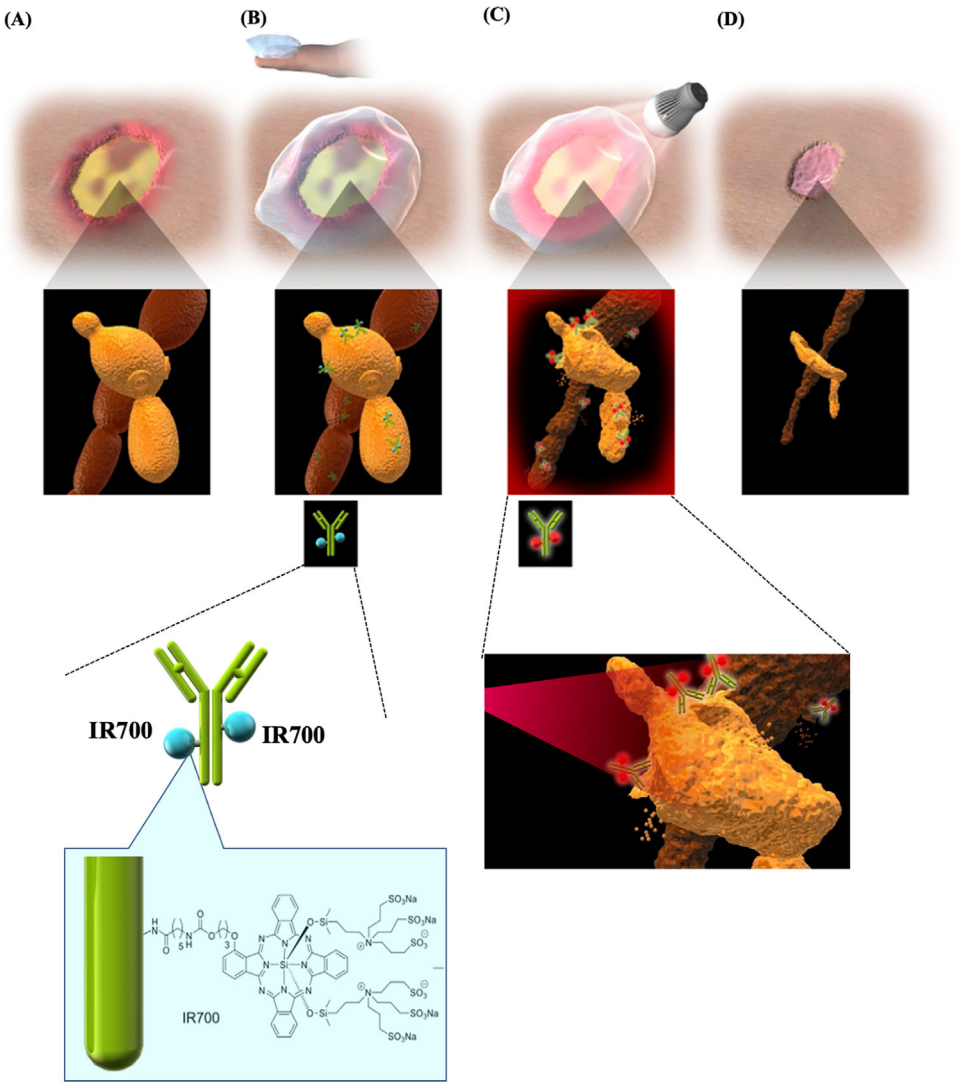

Figure 1. Schematic diagram depicting the mechanism of action of photo-antimicrobial targeting therapy (PAT^2). A) The infectious ulcer schema with pathogens at the bottom of the ulcer. B) IRDye700Dx (IR700) is applied to the infectious cutaneous ulcer to elicit a reaction between the pathogen and IR700. C) Irradiation with near-infrared-light at a 690-nm peak activates IR700 on the pathogens. D)Then, the PAT^2 destroys the pathogen. The killing of the pathogen ameliorates inflammation and promotes the healing of the infectious cutaneous ulcer.

from that in the control for the A431 cell line (Figure 3C). These data indicated that CA-IgY-IR700 widely binds to *Candida* spp. but not human cells.

2.4. The Effects of IgY-PAT^2 on CA In Vitro

To evaluate the effect of IgY-PAT^2 and different concentrations of CA-IgY-IR700 on CA, the concentration of CA-IgY-IR700 was evaluated at a range between 10 and 200 μg mL^{-1} using the same light dose (256 J cm^{-2}). The number of colonies decreased in a CA-IgY-IR700 concentration-dependent manner, and the effect of IgY-PAT^2 was highest at an antibody concentration of 200 μg mL^{-1} (Figure S2, Supporting Information). Based on these results, we set the CA-IgY-IR700 concentration to 200 μg mL^{-1} so that the survival rate of CA was the lowest. These data suggested that CA consumes much of the IgY, as fungus grow at faster rates than cancer cells.

To visually observe the reaction caused by IgY-PAT^2, we compared control (CA cells alone), CA-IgY-IR700, and IgY-PAT^2 groups using fluorescence microscopy. After adding CA-IgY-IR700 to the cultured CA, IR700 fluorescence was observed on the surface of CA. With NIR-light irradiation, IR700 fluorescence disappeared, and then, PI fluorescence, indicating cell death, was increased (Figure 3D). Next, to detect morphological changes in CA, scanning electron microscopy observations before and after IgY-PAT^2 treatment were performed. IgY-PAT^2 with CA-IgY-IR700 led to CA deformation and holes on the cell surface, even though neither the control nor CA-IgY-IR700 altered the cell shape (Figure 3E).

Next, to quantitate the antimicrobial effect on CA, both the number of colonies and dead cells were counted. Moreover, to

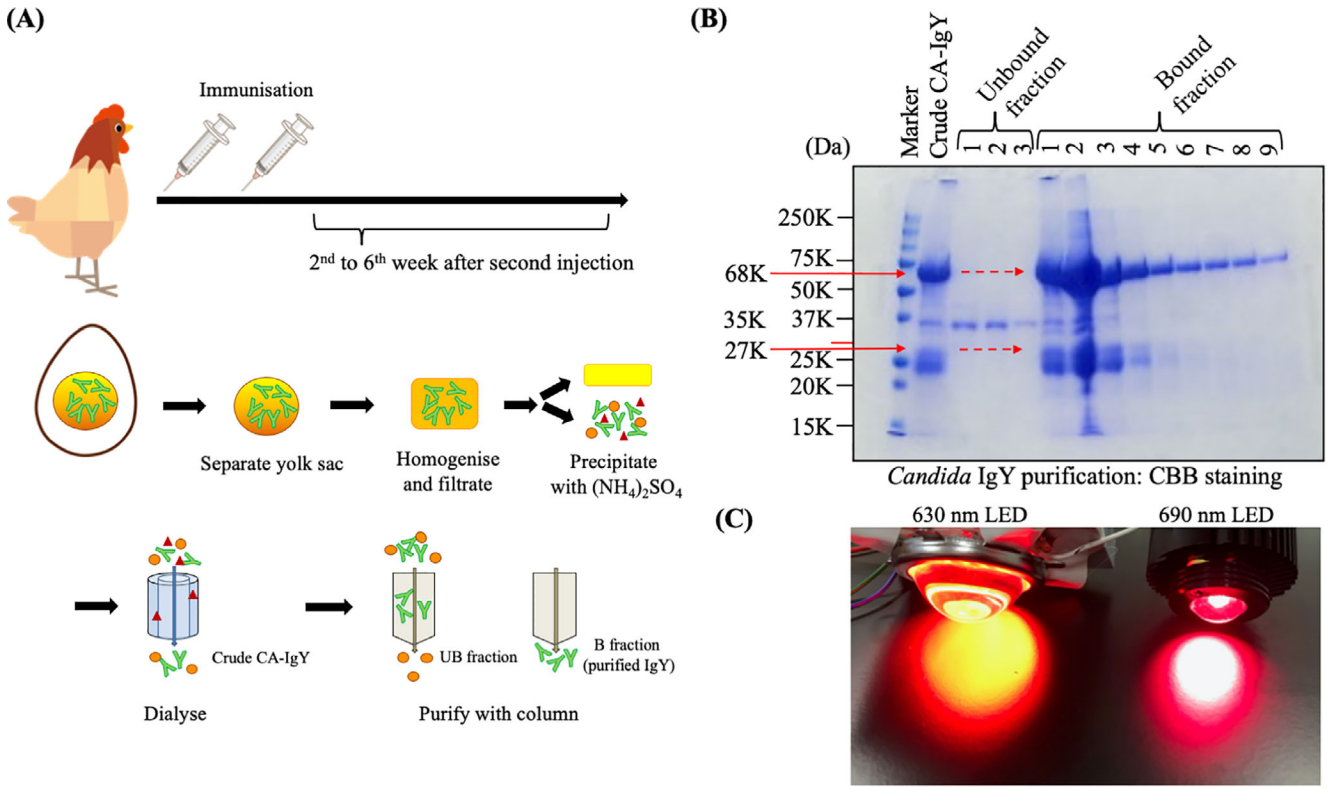

Figure 2. Production of anti-*C. albicans*-IgY (CA-IgY) and light sources. A) Scheme of the production of IgY-photo-antimicrobial targeting therapy (IgY-PAT_2). Hens were immunized by injection twice with inactivated *C. albincas*. Two to 6 weeks after second immunization, eggs were harvested daily. The collected yolks are homogenized and ammonium sulfate is added to collect the precipitate: partially purified IgY (Crude CA-IgY). Partially purified IgY is divided to unbound (UB) fraction and bound (B) fraction (means purified CA-IgY) with a thiophilic adsorbent column. B) SDS-PAGE of crude and CA-IgY fractions eluted from the column. The resolved proteins were stained with CBB. The bound fraction revealed IgY heavy chain bands at 68 kDa and IgY light chain bands at 27 kDa. The bands in all fraction at 35kDa might be the C-terminal fragment of the egg yolk protein vitellogenin II precursor. C) The light sources are shown; (left) a 630-nm wavelength (30 W red high-power LED; LED generic), and (right) a 690 nm high-power LED (L690-66-60; Usio-Epitex) were assembled. The 690 nm LED is set for PAT^2, 630 nm is for 5-ALA, respectively. CBB, Coomassie Brilliant Blue

compare both the photo-antimicrobial effect and mode of phototoxicity between conventional PDT and IgY-PAT^2, ALA-PDT was also examined. Since the antimicrobial effect of IgY-PAT^2 was supposed to be more rapid than that of ALA-PDT, we decided to count dead CA cells with propidium iodide (PI) staining and flow cytometry. IgY-PAT^2 caused fungal death via a photochemical reaction, whereas ALA-PDT exerted its effects via oxidative stress.[23] We also performed colony counting 1 day after therapy.

CA-IgY-IR700, IgY-PAT^2, and ALA-PDT induced a significant anti-fungal effect compared to those observed in the control group (CA cells alone). On comparing IgY-PAT^2 and CA-IgY-IR700, a significant difference was detected between 128J cm^{-2} and 256J cm^{-2}, indicating that IgY-PAT^2 exerts superior antimicrobial effects to only CA-IgY-IR700. Moreover, IgY-PAT^2 also exhibited a superior antimicrobial CA effect compared to ALA-PDT (**Figure 4**A).

With confirmation of the anti-fungal effect, next, we evaluated the speed of the effect. To detect a rapid antifungal effect, PI staining with flow cytometry was performed, which could detect necrotic and rapid death. With this rapid evaluation of antifungal effects, only IgY-PAT^2 induced anti-fungal effects, whereas neither CA-IgY-IR700 nor ALA-PDT showed any effects (Figure 4B). IgY-PAT^2 anti-fungal effects detected from 1 h after the light irradiation. On the other hand, ALA-PDT showed no effect from 1 to 6 h after the therapy (Figure S3, Supporting Information). Collectively, these results suggest that IgY-PAT^2 has an antimicrobial effect against CA in vitro and that the effect is more rapid than ALA-PDT, due to different phototoxicity mechanisms.[24]

2.5. In Vivo Antimicrobial Effect of IgY-PAT^2

To examine the effects of IgY-PAT^2 in vivo, we developed a skin-ulcer infection mouse model. Administering CA-IgY-IR700 onto the ulcer with an adhesive bandage, IR700-fluorescence was detected with a fluorescence imager on day 1 before irradiation, as well as day 3, 5, and 7. On day 1, IR700-fluorescence was observed on the ulcer area, which is covered with an adhesive bandage, suggesting that CA-IgY-IR700 attached to the ulcer area. On day 3, after NIR-light irradiation, IR700-fluorescence disappeared in the PAT^2 group, whereas in the CA-IgY-IR700 group (no NIR-light irradiation), the IR700-fluorescence of the ulcer area remaining until day 7, indicating that CA-IgY-IR700 attached to the CA in the infectious ulcer (**Figure 5**A). The appearance of NIR-light irradiation in the mouse model is shown in Figure 5B. These

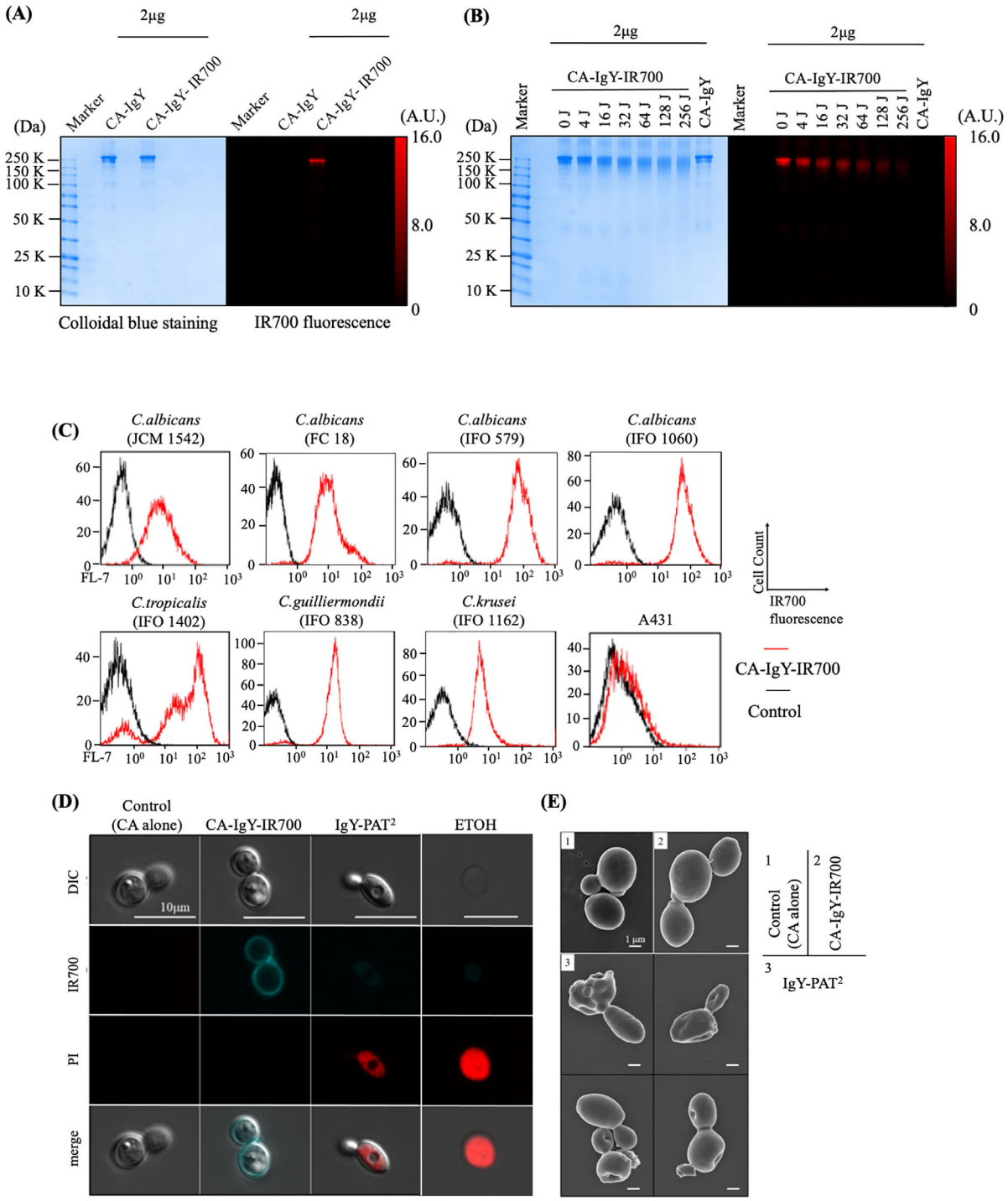

Figure 3. Production and evaluation of CA-IgY-IR700 (IRDye700Dx) and in vitro observation of photo-antimicrobial targeting therapy (PAT^2). A) Conjugation of CA-IgY and IR700 and the validation of CA-IgY-IR700 by SDS-PAGE (left: colloidal blue staining (protein staining), right: fluorescence at 700 nm). B) The CA-IgY-IR700 was irradiated with near-infrared (NIR) light and electrophoresed by SDS-PAGE. The protein bands become thin with a smear over its protein band along with loss of IR700-fluoresence. C) Flow cytometric analysis of CA-IgY-IR700 in various *Candida* spp. and A431 cells. CA-IgY-IR700 was not added to the control. CA-IgY-IR700 reacted with various *Candida* spp., whereas fluorescence was absent in the A431 cells. D) Fluorescence microscopy observations of *C. albicans* (CA) incubated with CA-IgY-IR700 and irradiated with NIR-light IgY-PAT^2 treatment. CA cells were cultured with CA-IgY-IR700 for 4 h and then irradiated with NIR-light (256 J cm^{-2}). CA-IgY-IR700 was detected on the surface of CA. Upon IgY-PAT^2 treatment, CA was stained with propidium iodide (PI: necrotic cells are stained) under the condition that CA treated with ethanol (positive control) was also stained. E) The surface of CA was observed with a scanning electron microscope. No change in the cell surface could be confirmed in (1) control and (2) CA-IgY-IR700 conditions. In response to (3) IgY-PAT^2, the PAT^2-treated CA surface was disrupted or deformed. DIC, differential interference contrast; ETOH, ethanol

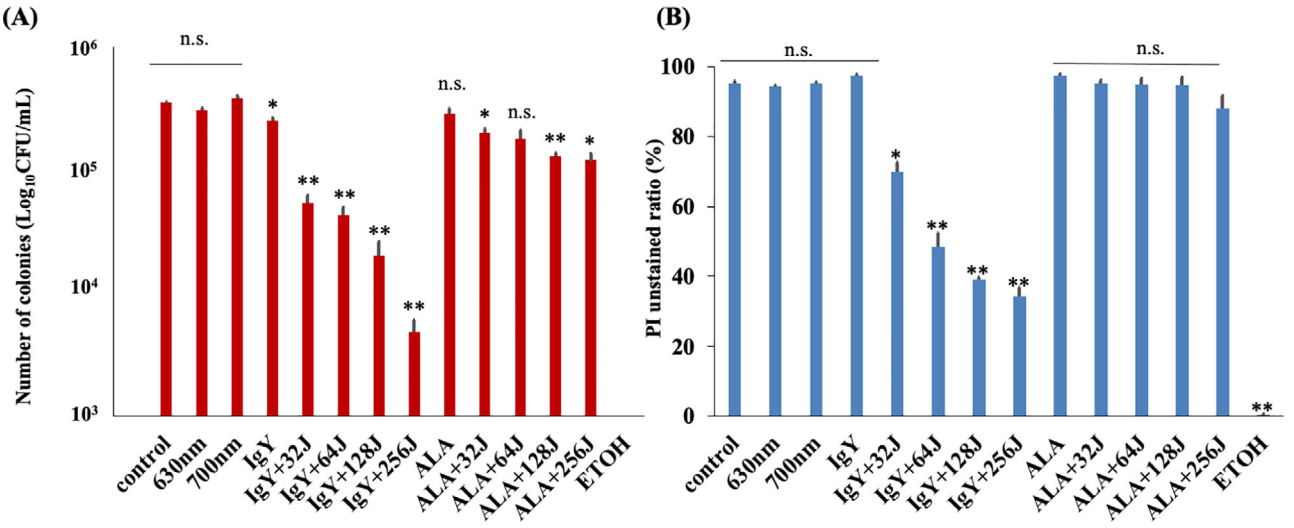

Figure 4. Effects of IgY-PAT^2 (photo-antimicrobial targeting therapy) and aminolaevulinic acid- photodynamic therapy (ALA-PDT) against *C. albicans* (CA) in vitro. For each result, CFUs count and flow cytometer are performed by the following method: cell alone (control), light without photosensitizer (630 or 690 nm), photosensitizer without light (ALA or CA-IgY-IR700 (IRDye700Dx), photosensitizer and light (IgY-PAT^2 or ALA-PDT). A) In vitro effects of IgY-PAT^2 and ALA-PDT on CA, as measured by colony counts. The CFU ratio significantly decreased in the CA-IgY-IR700, IgY-PAT^2, and ALA-PDT groups, and IgY-PAT^2 or ALA-PDT effects occurred in an irradiation dose-dependent manner. When comparing the in vitro effects between IgY-PAT^2 and ALA-PDT at the same dose, effects of IgY-PAT^2 were superior to those of ALA-PDT (control versus CA-IgY-IR700: $p = 0.0007$; control versus IgY-PAT^2: $p = 0.0012$ at 32 J cm^{-2}, 0.0054 at 64 J cm^{-2}, 0.0093 at 128 J cm^{-2}, 0.0046 at 256 J cm^{-2}; CA-IgY-IR700 versus IgY-PAT^2: $p = 0.0026$ at 32 J cm^{-2}, $p = 0.0112$ at 64 J cm^{-2}, $p = 0.0135$ at 128 J cm^{-2}, $p = 0.0067$ at 256 J cm^{-2}, control versus ALA-PDT: $p = 0.0429$ at 32 J cm^{-2}, 0.180 at 64 J cm^{-2}, 0.0013 at 128 J cm^{-2}, 0.0132 at 256 J cm^{-2}; IgY-PAT^2 versus ALA-PDT: $p = 0.0020$ at 32 J cm^{-2}, 0.0209 at 64 J cm^{-2}, 0.0243 at 128 J cm^{-2}, 0.0289 at 256 J cm^{-2}). Data are means ± SEMs ($n = 6$, $p < 0.0001$, $F = 283.5$, degrees of freedom (DF) = 83 [ANOVA], $*p < 0.05$, $**p < 0.001$ [Tukey's-test]). B) In vitro effects of IgY-PAT^2 and ALA-PDT on CA, flow cytometer was performed after 3 h of light irradiation with propidium iodide (PI). To directly compare the results of colony counting, the proportions of PI-unstained (live) CAs are shown. With respect to the in vitro effects of IgY-PAT^2 and ALA-PDT, only the IgY-PAT^2 group showed obvious effects, whereas the others did not show any difference relative to the control (control versus IgY-PAT^2: $p < 0.0001$ at 32–256 J cm^{-2}; CA-IgY-IR700 versus IgY-PAT^2: $p < 0.0001$ at 32–256 J cm^2). The in vitro effects of IgY-PAT^2 on PI staining were increased in a near-infrared-light dose dependent manner. Data are means ± SEMs ($n = 3$, $p < 0.0001$, $F = 95.02$, DF = 50 [ANOVA], $*p < 0.05$, $**p < 0.001$ [Tukey's-test]). IgY means CA-IgY-IR700 in the figure.

data suggested that the IR700-fluorescence could be a guide for NIR-light irradiation and that its decrease marks the completion of therapy. The representative appearance of an ulcer or infectious ulcers is shown in Figure 5C. As shown, purulent discharge was often observed in the CA and light group, suggesting that infection progressed and enhanced inflammation occurred. Epithelialization had almost finished on day 9 in the no infection control group based on the natural course of recovery. Under these conditions, epithelialization had not yet completed on day 13 in the CA and light group mice. Infectious ulcers exhibited almost completed epithelialization on day 13 in the CA-IgY-IR700 group mice. However, epithelialization was almost completed by day 11 in the PAT^2 group mice. Neither the light nor the IgY-PAT^2 group have apparent side effects related to NIR-irradiation such as burns (Figure 5C). To quantitatively evaluate IgY-PAT^2 in vivo, the ulcer area was measured using calipers. The non-infection control group mice had the smallest ulcer area. Under these conditions, IgY-PAT^2 group mice showed a significant reduction in the infectious ulcer area compared to that in the other groups. After day 7, the ulcer area in the IgY-PAT^2 group mice was almost the same as that in the non-infection control mice (Figure 5D). Based on detailed analysis, the ulcer area in the CA-IgY-IR700 group mice was smaller than that in the CA group; however, there was no statistical difference. The light group did not differ from the CA group on all days. Next, to evaluate the microbiological effect of IgY-PAT^2, the number of colonies in the ulcer area was evaluated. The IgY-PAT^2 group had fewer colonies than the CA group and this was equivalent to that in the non-infection control group, suggesting that IgY-PAT^2 exert almost a complete anti-fungal effect on the CA infectious ulcers (Figure 5E).

2.6. In Vivo Inflammation Evaluation Based on Cytokines

To evaluate the inflammatory status in vivo in the infectious ulcer mouse model, cytokines in the ulcer area were examined in the no infection, CA infection, and IgY-PAT^2 groups. As a standard based on the non-infection control mice, comparative analysis between CA and IgY-PAT^2 mouse groups was performed (**Figure 6** and Figure S4, Supporting Information). As CA infection caused a high level of inflammation in the ulcer area, the inflammatory cytokine levels were higher than those in IgY-PAT^2 group mice (based on IL-1α, IL-1β, TNFα, IFN-γ, LIF, MIP-1α, MIP-1β, MIP-2, RANTES, VEGF, PLEG-2, G-CSF, SDF-1). These anti-inflammatory effects of IgY-PAT^2 may be the result of its excellent photo-microbial effect as well as its selectivity toward CA. Moreover, to validate the relationship between inflammatory cytokines or chemokines and bacterial infection status, we performed correlation analysis across all groups in vivo. Almost all cytokines exhibited some correlations, and among them,

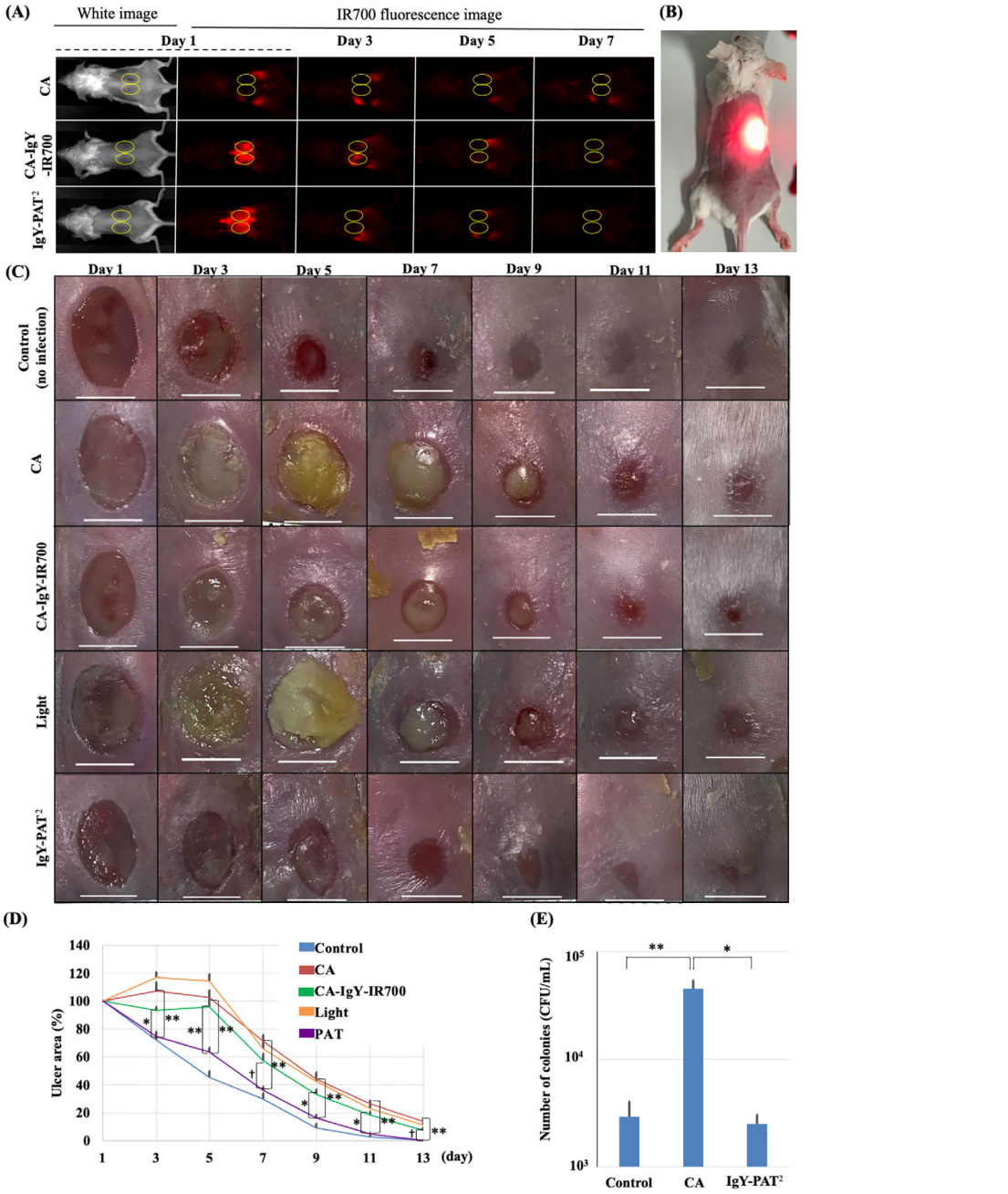

Figure 5. In vivo effects of photo-antimicrobial targeting therapy (PAT^2) on mouse cutaneous infection models. A) Representative fluorescence images comparing the *C. albicans* (CA), CA-IgY-IR700 (IRDye700Dx), and IgY-PAT^2 (700 nm fluorescence) groups. CA-IgY-IR700 was detected as IR700-fluorescence at the site where the adhesive bandage containing the CA-IgY-IR700 was attached to the infected ulcer area. At day 3 after near-infrared (NIR)-light irradiation, the IR700-fluorescence almost completely disappeared in the IgY-PAT^2 group. However, the IR700-fluorescence in the ulcer area remained until day 7 in the CA-IgY-IR700 group (no NIR-light irradiation, only CA-IgY-IR700). The ulcer areas are enclosed by a yellow circle. B) A picture of an NIR-light irradiated mouse. C) Representative photos of the ulcers in mice from each group. Control ulcers were not infected with CA. Abundant purulent excretion was detected in the CA group and light group, whereas this was markedly diminished in the control (no infection) and IgY-PAT^2 groups. The white line indicates 5 mm. D) The in vivo effects of IgY-PAT^2 on mouse cutaneous infection models, as measured based on ulcer areas. In the IgY-PAT^2 group, significant ulcer reduction was observed compared to that in the CA groups (IgY-PAT^2 versus CA: $p = 0.0002$ at day 3, 0.0004 at day 7, < 0.0001 at day 13; IgY-PAT^2 versus CA-IgY-IR700: $p = 0.0497$ at day 3, 0.0505 at day 7, 0.0664 at day 13). The IgY-PAT^2 group exhibited almost the same level of ulcer reduction as the control (no infection) group, and no significant change was detected (IgY-PAT^2 versus control: $p = 0.9961$ at day 3, 0.9194 at day 7, 0.6628 at day 9, > 0.9999 at day 13). The ulcer area of the CA-IgY-IR700 group was smaller than that of the CA group. The light group showed no significant difference from the CA group. Data are means ± SEMs ($n \geq 7$, $\dagger p < 0.1$, $*p < 0.05$, $**p < 0.001$, [Tukey's test]). E) Confirmation of colony counting from infected cutaneous ulcers. A comparison of the number of yeasts in the ulcer tissue on day 2 is shown. The numbers of colonies were significantly decreased in the control (no infection) and IgY-PAT^2 groups. Data are means ± SEMs ($n \geq 3$, $p = 0.0073$, $F = 9.698$, DF = 10 [ANOVA], $*p < 0.05$, $**p < 0.001$ [Tukey's test]).

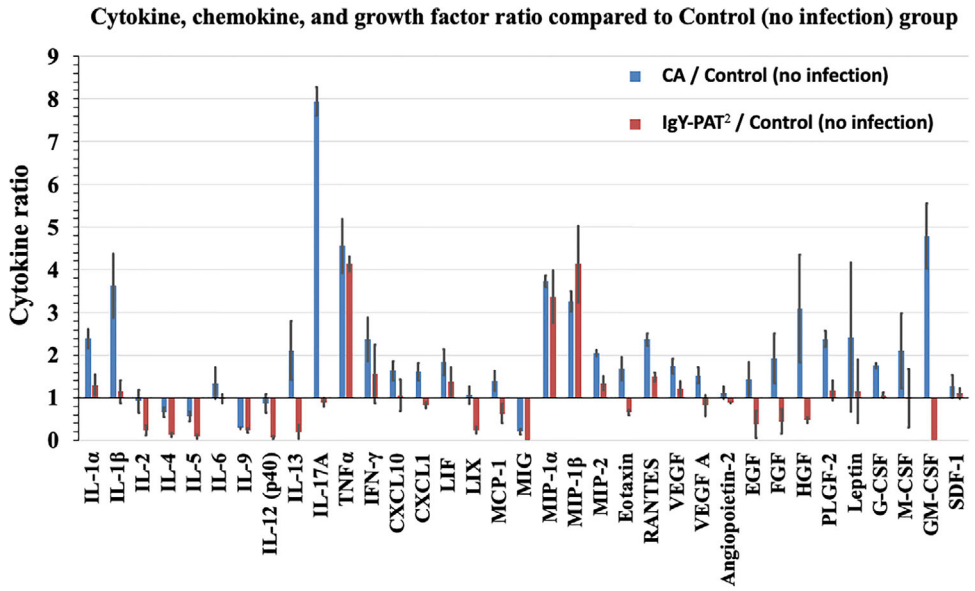

Figure 6. Examination of the effect of IgY-PAT^2 (photo-antimicrobial targeting therapy) on in vivo inflammation based on mouse cutaneous infection models. The ratios of cytokines and chemokines in the CA and IgY-PAT^2 groups, based on the standard of the control (no infection) group, are shown. Data are means ± SEMs ($n = 3$).

IL-17A and IL-1β showed especially strong correlations with the number of CFUs (Figure S5, Supporting Information), suggesting that these data were in accordance with the infection status. Together with these results, IgY-PAT^2 promoted healing in the mouse model of CA-infected cutaneous ulcers, and the condition was restored to the same level as observed in the no infection control group.

3. Conclusion

New antibacterial drugs have been created to overcome the drug-resistant bacteria problem but their efficacy does not last very long because pathogenic bacteria can develop resistance against them quickly. Antibacterial drugs can be roughly classified into the following five classes based on their mechanisms of action: inhibitors of DNA synthesis, cell wall synthesis, folic acid synthesis, and ribosomal RNA subunits and mediators of changes in cell membrane permeability.[25] Beyond these conventional mechanisms, photo-activated antimicrobial therapy has the potential to become a new modality to combat infectious diseases. However, conventional PDT for bacteria, which is known as photodynamic antimicrobial chemotherapy, has no targeting ability and thus damages normal human cells. In fact, photosensitivity after PDT is a frequent side effect.[26] These limitations can be attributed to the mechanisms of action of conventional PDT,[24] which involve the generation of oxidative stress (via reactive oxygen species) resulting in less targetable apoptosis. However, PAT^2, a modified form of NIR-PIT depends on the rapid necrotic cell death caused by photo-chemical reactions[27,28] and thus could become the next ideal photo-antimicrobial therapy. With this new mechanism, which results in photo-damage to the cell wall or membrane, the bacteria or fungi are subjected to irreversible necrotic damage. This process is suggested to be less likely to result in the development of resistance against therapy because drug uptake and metabolism are irrelevant (Figure S6, Supporting Information).

In terms of the light therapy, NIR-PIT is composed of a targeting antibody, IR700, a photoabosorber, and light sources. These three elements must be optimized to realize the best therapy. Although a monoclonal antibody was originally used for NIR-PIT for cancers,[8,29] we exploited polyclonal IgY to develop PAT^2. In cancer therapy, monoclonal antibodies are used to precisely distinguish between human normal cells and tumor cells,[8,30,31] since they are very similar to each other; in other words, the cancer cells were originally derived from normal cells. However, fungus have cell walls containing many components such as mannoproteins that are not found in human cells, which lead to bigger differences in antibody recognition. Based on these considerations, polyclonal antibodies could be used in PAT^2 with no particular difficulties. Moreover, polyclonal antibodies can target a variety species in the same family of fungus with "similar" antigens. Indeed, in this study, cross-reactivity with CA-related species was determined, and this might be a great advantage for the treatment of infectious diseases caused by fungus such as *Candida auris*, an emerging multidrug-resistant pathogen.[32] Another advantage of using polyclonal IgY is the lower cost to generate the antibodies. Compared to cancer cells, pathogens grow more drastically under good condition.[33,34] Since antibody consumption during therapies for infection is increased and occurs at a faster rate compared to that during cancer therapies, PAT^2 requires high concentrations of antibodies. To satisfy this demand, a large quantity of antibodies is needed, and thus, IgY could be cost-saving for use as material for PAT^2.

Another main component of this therapy is NIR-light. NIR-light has better tissue penetration than other wavelengths, because this range of light is absorbed less by water and hemoglobin.[8] We used a high-power LED or laser to treat the mouse cutaneous infection models. In clinical use, we intend to

use medical laser devices to ablate the pathogens from the infection area. We can apply these therapies with no limitations in the cumulative irradiation dose of NIR-light, as this is not ionizing radiation such as X-rays. Therefore, we can perform therapy repeatedly until the targeted pathogens are completely eliminated. Moreover, device development with endoscopies or catheters could enable NIR-light to be delivered anywhere in the body in the near future.

The CA-targeting IgY-PAT^2 resulted in highly selective damage to CA in vivo, as evidenced by the low levels of most cytokines and chemokines in the IgY-PAT^2 group than those in the CA group. If the PAT^2 had damaged normal skin cells, the resulting inflammation would have led to the development of additional infectious epithelialized ulcers. Highly selective damage controlled by both IgY and light sources would lead to the prompt ablation of CAs without damaging epithelial cells, resulting in almost the same level of recovery as that in the no infectious control ulcers. We only used PAT^2 in the skin; however, theoretically, PAT^2 could have the same effect anywhere in the body.

This study has some limitations. First, we have not examined ALA-PDT in detail. We just want to compare the in vitro effects with different photo-reactive mechanisms.[28,35,36] Second, the therapeutic effect is determined only with specific antibodies and *Candida spp*. It is necessary to study with other pathogens and antibodies in the future. Third, high doses of IgY can cause adverse events such as anaphylaxis or egg allergy. It is necessary to stabilize and optimize antibody reactivity and specificity by improving the antibody purification method.

IgY-PAT^2 is expected to have the following applications. Devices such as optic fiber for NIR irradiating inside the body have been reported.[37–39] The antibody is administered externally, orally, by enema, or by intravenous administration, and then NIR irradiation is applied to any site. Therapeutic applications for skin diseases such as ringworm, oral diseases, gastrointestinal infections such as *H. pylori*, and abscesses are considered. Further, the antibody can be cloned easily, or human monoclonal antibody specific to the pathogen can be used.

In conclusion, we developed a new NIR-activated IgY-PAT^2 method for controlling *Candida* infections by using IR700 to conjugate anti-*Candida* IgY antibodies. CA-targeting IgY-PAT^2 led to recovery in a cutaneous infectious mouse ulcer model to almost the same extent as that observed in the no infection control group. The effects of IgY-PAT^2 were prompt and resulted in almost no damage to the epithelia. The IR700-fluorescence of the photoabsorber in the conjugates could be used as a noninvasive guide for the therapeutic area and as a biomarker to confirm the therapeutic effects. Further, we could change the target pathogens by changing the IgY, suggesting that PAT^2 would serve as a universal anti-infection platform.

4. Experimental Section

Reagents: Water-soluble, silica-phthalocyanine derivative IRDye 700DX NHS ester was purchased from LI-COR Biosciences (NB, USA). CA-IgY was obtained from Immunology Research Institute (Gifu, Japan). All other chemicals were of reagent grade.

Immunization with CA and Purification of CA-IgY: For the production of IgY, 18-week-old Hy-Line hens were immunized by intramuscular injection of an emulsified mixture of inactivated CA and oil emulsion. Eggs laid by the immunized hens between 2 and 6 weeks after second immunization were harvested and egg yolk was isolated, pooled and processed into powder form in accordance with a method described previously.[40] IgY antibodies were partially purified from the egg yolk powder by chloroform extraction and ammonium sulfate precipitation.[41] This partially purified freeze-dried powder IgY (crude IgY) was further purified by Pierce Thiophilic Adsorption Kit (Thermo Fisher Scientific, MA, USA). This protocol was carried out as per manufacturer's guidelines. The eluted protein fractions were pooled. All purifications were carried out at 15–25 °C. The purity and composition of all fractions were analyzed by SDS-PAGE under reducing conditions as described by Laemmli.[42] The resolved proteins were stained with BioSafe Coomassie (BioRad, CA, USA) for 1 h. The total protein concentration of column fractions was measured by spectrophotometry at 280 nm (Thermo Scientific NanoDrop Lite; Thermo Fisher Scientific). The total IgY concentrations were determined using sandwich ELISA quantification kits (Bethyl Laboratories, TX, USA) following the manufacturer's instructions. The purified IgY was designated as CA-IgY.

Synthesis of IR700-conjugated CA-IgY: CA-IgY (1 mg, 5.4 nmol) was incubated with IR700 (47.8, 24.5 nmol, 10 mmol L^{-1} in DMSO) and 0.1 mol L^{-1} Na_2HPO_4 (pH 8.6) at 15–25 °C for 1 h. The mixture was purified using a Sephadex G50 column (PD-10; GE Healthcare, NJ, USA). Protein concentration was determined using a Coomassie Plus protein assay kit (Thermo Fischer Scientific) by measuring the absorbance at 595 nm through spectroscopy (UV9100; SHIMADZU, Kyoto, Japan).

The concentration of IR700 was measured based on the absorbance at 689 nm via spectroscopy to confirm the number of fluorophore molecules conjugated to CA-IgY. The synthesis was controlled so that an average of three IR700 molecules were bound to a single IgY. SDS-PAGE was performed as a quality control for each conjugate in accordance with a previously reported method.[8,43] Diluted CA-IgY was used as nonconjugated controls for SDS-PAGE and the fluorescent bands were measured with Pearl Trilogy (LI-COR Biosciences) using a 700-nm fluorescence channel.[44]

Candida Culture: CA (JCM 1542) was obtained from Immunology Research Institute, EW Nutrition Japan. CA (FC 18) was collected from patients at the University Hospital.[45] CA (IFO 579, IFO 1060), *Candida tropicalis* (IFO 1402), *Candida guilliermondii* (IFO 838), and *Candida krusei* (IFO 1162) were obtained from the Institute for Fermentation, Osaka (Oyodogawa, Osaka, Japan). *Candida* spp. were cultured by suspension in SD medium (2 % glucose (NAKALAI TESQUE, Kyoto, Japan), 0.5 % $(NH_4)_2SO_4$ (Becton Dickinson, NJ, USA), 0.17 % yeast nitrogen base without amino acids and $(NH_4)_2SO_4$ (Becton Dickinson)) in tissue culture flasks in a shaking incubator at 30 °C at 150 rpm. Candida spp. were used for experiments after cultivated in the SD medium at least 24 h.

Cell Culture: A431 cells (CRL-1555; American Type Culture Collection, VA, USA) were cultured in RPMI 1640 medium (Thermo Fisher Scientific, MA, USA) supplemented with 10 % fetal bovine serum and penicillin (100 IU mL^{-1})-streptomycin (100 mg mL^{-1}) (Thermo Fisher Scientific) in a tissue culture dish at 37 °C in a humidified incubator with an atmosphere of 95% air and 5% carbon dioxide.

Flow Cytometry: To verify in vitro CA-IgY-IR700 binding, the fluorescence was measured from CA after incubation with CA-IgY-IR700 with a flow cytometer.

First, the CA-IgY-IR700 concentration was determined. 1.0 x 10^5 CA (JCM 1542) were seeded into a 1.5-mL microcentrifuge (MCT); then CA-IgY-IR700 (1 mg mL^{-1}) and SD medium were added so that the total amount was 1 mL, and CA-IgY-IR700 was adjusted to 0–500 μg mL^{-1}. After incubation at 37 °C for 1 h in absence of light, the 700 nm fluorescence from CA was measured and analyzed using a flow cytometer (Gallios; Beckman Coulter, CA, USA) with Kaluza software (Beckman Coulter) (Figure S1, Supporting Information). Considering the amount of CA-IgY-IR700 that can be used, the following experiments were performed at 200 μg mL^{-1}. It was confirmed that the fluorescence intensity increased in a concentration-dependent manner. Considering the amount of antibody that can be used, the following experiments were performed at 200 μg mL^{-1}.

To evaluate other Candida spp. and human cell, the fluorescence from CA (IFO 579, IFO 1060, and FC18), related species (*C. tropicalis*, *C. guilliermondii*, and *C. krusei*) and A431 was evaluated in the same manner. A431 cells (1.0×10^5) were cultured in 12-well plates and incubated for 24 h, then CA-IgY-IR700 and RPMI 1640 medium were added so that the total amount was 1 mL, and CA-IgY-IR700 was adjusted to 200 μg mL^{-1}. CA-IgY-IR700 was not added to the control.

In Vitro ALA-PDT: For this assay, 1.0×10^5 CA (JCM 1542) cells in culture medium were taken into 1.5-mL MCTs, and treated with 0.5% ALA to the culture medium to reach a final volume of 1 mL, which was incubated at 30 °C for 4 h with light shielding.[46] CA/ALA was irradiated with LED at a wavelength of 600–640 nm (30 W red high-power LED; LED generic, Yamanashi, Japan) at a power density of 100 mW cm^{-2} as measured by an optical power meter (PM100; Thorlabs, NJ, USA). The tubes were placed on ice to protect them from heat during the LED irradiation.

In Vitro IgY-PAT²: For this, 1.0×10^5 CA (JCM 1542) were seeded into 1.5-mL MCTs, and 10–200 μg mL^{-1} CA-IgY was added to the culture medium to reach a total volume of 1 mL, which was incubated at 30 °C for 4 h with light shielding. CA/CA-IgY-IR700 was irradiated at a wavelength of 670–710 nm using a laser (MLL-III-690nm Laser, CNI Laser, Changchun, China) or LED (L690-66-60; Usio-Epitex, Kyoto, Japan) at a power density of 100 mW cm^{-2}.

Cell Viability Assay Using Microscopy: To detect the antigen-specific localization of the IR700 conjugate, observation with a fluorescence microscope was performed (A1Rsi; Nikon, Tokyo, Japan). CA (JCM 1542) was incubated with IgY-PAT² at room temperature for 3 h, washed with PBS. As a dead cell control, CA was treated with 70% ethanol for 15 min and washed with PBS. A thousand CA cells were seeded onto poly-D-lysine-coated 3.5-mm glass bottom dishes. Propidium iodide (PI; final concentration, 1 μg mL^{-1}; Thermo Fisher Scientific) was added into the medium 30 min before the observation to detect membrane- and cell wall-damaged CA (i.e., dead CA).

Scanning Electron Microscopy: To detect a change in the surface structure, electron microscopy was performed. CA (JCM 1542) was harvested at 15–25 °C 3 h after IgY-PAT² treatment and was then washed with PBS. CA cells were fixed in 2 % glutaraldehyde (TAAB Laboratories Equipment, Berks, UK), at 4 °C for 24 h and then washed with PBS for 15 min and fixed again in 1% osmium tetroxide (TAAB Laboratories Equipment) at 4 °C for 2 h. Ethanol was used at increasing concentrations (50%, 60%, 70%, 80%, 90%, 95%, and 99%; 10 min each) to dehydrate the samples. CA was replaced with t-butyl alcohol and lyophilized (VFD-21S; Vacuum Device, Ibaraki, Japan). Then, cells were coated with osmium plasma (NL-OPC80NS; Japan Laser, Tokyo, Japan) and observed under a scanning electron microscope (JSN-7610F; Japan Electronic Optics Laboratory, Tokyo, Japan).

Comparison Between IgY-PAT² and ALA-PDT: To compare the antimicrobial effects of IgY-PAT² and ALA-PDT on CA, the following groups were used: CA cells alone (control group), CA with irradiation 630 or 690 nm light without photosensitizer (light group), CA with photosensitizer without light (IgY or ALA), CA with photosensitizer and irradiation (IgY-PAT² or ALA-PDT). The dead cell control was treated with ethanol for 4 h and washed with PBS (ETOH). The light group was subjected to a light-dose of 256 J cm^{-2} (maximum dose), and IgY-PAT² and ALA-PDT groups were irradiated at a range from 32 to 256 J cm^{-2}. To confirm the proportion of surviving CA (JCM 1542) cells, the colony forming units (CFUs) were counted. CA cells were diluted 10^3- to 10^4-fold and plated on sterile YPD agar medium (2 % glucose, 2 % polypeptone (Becton Dickinson), 1 % yeast extract (Becton Dickinson), and 2 % agar (Becton Dickinson)) immediately after IgY-PAT² treatment. The number of CFUs with 30–300 colonies per plate was counted visually after incubation at 30 °C for 24 h. In addition, to determine the destruction ratio of CA by IgY-PAT² and ALA-PDT, the proportion of PI staining was examined by flow cytometry (FACS Calibur, BD BioSciences) using CellQuest software (BD BioSciences) 3 h after irradiation at room temperature.

Mouse Model of CA-Infected Cutaneous Ulcers: All in vivo procedures were conducted in compliance with the local Animal Care and Use Committee of Nagoya University (Approval Number, 2019-31431, 2020-20104). For this model, 8–10-week-old female BALB/c SLc mice were purchased from Chubu Kagaku Shizai (Aichi, Japan). The animals were housed at six per cage and maintained under a 12-h light/dark cycle with ad libitum access to food and water. During the procedures, mice were anaesthetized with isoflurane (Wako). The back was shaved with an electric razor, and a depilatory agent was used.

On the back of each mouse, a 6-mm punch biopsy tool was used to create full-thickness skin defects (6 mm in diameter) that extended through the panniculus carnosus. Two ulcers were made on each mouse, with an ulcer on each side of the midline back. CA (JCM 1542) cells were washed with PBS and diluted to 10^9 CFU mL^{-1} with 100 μL PBS; an adhesive bandage (band-aid junior type, Johnson & Johnson, NJ, USA) was soaked in this suspension and attached to the ulcer. Ulcers in the control group were bandaged using bandages soaked in PBS. Next, a dressing (meshpore tape; Nichiban, Tokyo, Japan) was wrapped around each animal to protect the shaved skin and the ulcers. This state was maintained for 1 day to generate the mouse model of CA-infected cutaneous ulcer.

An ointment was prepared by mixing water-soluble jelly (luve-jelly; Japan family planning association, Tokyo, Japan), PBS, and CA-IgY-IR700 and finally doubling the jelly volume so that CA-IgY-IR700 was present at a concentration of 200 μg mL^{-1} (IgY ointment). An ointment without CA-IgY-IR700 was also prepared (PBS ointment). 1 day after infection, the adhesive bandages and a dressing were replaced with other adhesive bandages soaked in 100 μL CA-IgY-IR700 or PBS ointment, and another dressing. This condition was maintained for 1 day.

In Vivo IgY-PAT²: To evaluate the effect of IgY-PAT² in vivo on CA-infected cutaneous ulcers, therapeutic efficacy was compared among the five groups. The control group (no infection, asepsis) included mice without infection (only cutaneous ulcers without infection). The other groups were infected and treated as follows: the CA group had cutaneous ulcers with CA-infection without treatment, the IgY group had CA-infected cutaneous ulcers with CA-IgY-IR700 but without NIR-light irradiation, the light group had CA-infected cutaneous ulcers with only NIR-light irradiation, and the IgY-PAT² group had CA-infected cutaneous ulcers with CA-IgY-IR700 and NIR-light irradiation.

Day 1 was defined as the NIR-light irradiation day (2 days after the cutaneous ulcers were created and inoculated with CA, and 1 day after the ointment was applied). The mice were irradiated with laser at a wavelength of 670–710 nm (MLL-III-690nm Laser, CNI Laser) up to 256 J with 100 mW cm^{-2} output. After irradiation, the bandages were replaced with new ones, and then, the ulcer was observed and the bandage was changed every other day until day 13. The size of the wound area was measured by tracing the wound margin and calculating the area in pixels using ImageJ 1.52a (National Institutes of Health, MD, USA). The area of the ulcer on day 1 was 100%; 0% indicates that the ulcer was completely epithelialized. At least nine ulcers were analyzed in each group.

Yeast Counting in Wound Tissue for CA-Infected Cutaneous Ulcers In Vivo: It was microbiologically evaluated whether IgY-PAT² has an antimicrobial effect in vivo. On day 2 (1 day after NIR irradiation), a part of the ulcer (5 mm in diameter) was excised aseptically to the level of the deep fascia using 5-mm punch biopsy for the asepsis, CA, and IgY-PAT² groups ($n \geq 3$). The ulcer samples were homogenized in 1 mL of PBS. Viable yeasts in PBS were counted by making tenfold serial dilutions and culturing the dilutions on YPD agar at 30 °C for 24 h; at least three ulcers were tested in each group.

Cytokine Measurements: Similar to the microbiological evaluation (yeast counting), the cytokines in the ulcer area were evaluated in the same manner. On day 2 (1 day after NIR irradiation), the ulcer tissue was removed using the same method among asepsis, CA, and IgY-PAT² groups ($n \geq 3$). The ulcer samples were homogenized in 1 mL of PBS supplemented with protease inhibitors (cOmplete Tablets; Sigma-Aldrich, MO, USA), and then, the solution was passed through a filter (Cell Strainer 70 μm Nylon; CORNING, NY, USA) and cryopreserved at −80 °C.[10] the solutions were kept frozen and sent to Eve technologies (Calgary, Canada) for cytokine measurement which was performed by using a Mouse Cytokine Array/Chemokine Array and Angiogenesis Featured Array.

Statistical Analysis: Data were expressed as means ± SEMs from a minimum of three experiments. Statistical analyses were performed with a statistics program (GraphPad Prism; GraphPad Software, CA, USA). For multiple-group comparisons, a 1 way ANOVA with Tukey's test was used. The statistical tests used two-tailed.

Supporting Information

Supporting Information is available from the Wiley Online Library or from the author.

Acknowledgements

H.S. and K.S. contributed equally to this work. The authors would like to thank all the members of their laboratory and section for their comments and suggests on this research. The authors also thank to the nano-plat form at Nagoya University, and core technical staffs in Nagoya University Equipment Sharing System. This research was supported by the Program for Developing Next-generation Researchers (Japan Science and Technology Agency), KAKEN (18K15923, JSPS), Toukai Foundation for Technology, GSK Japan Research Foundation, Hyper Interdisiplinary Conference Research Award, Uehara Infection/Chemotherapy Research Award. Funders only provided funding, and had no role in the study design, data collection, data analysis, interpretation, and writing of the report.

Conflict of Interest

The authors declare no conflict of interest.

Keywords

Candia albicans, IR700Dx, near infrared photoimmunotherapy, PAT^2, photo-antimicrobial therapies

Received: October 5, 2020
Revised: November 16, 2020
Published online:

[1] J. Carlet, C. Pulcini, L. J. V. Piddock, *Clin. Microbiol. Infect.* **2014**, *20*, 949.
[2] H. W. Boucher, G. H. Talbot, J. S. Bradley, J. E. Edwards, D. Gilbert, L. B. Rice, M. Scheld, B. Spellberg, J. Bartlett, *Clin. Infect. Dis.* **2009**, *48*, 1.
[3] A. K. Janson, C. I. E. Smith, L. Hammarström, in *Advances in Experimental Medicine and Biology*, (Eds: J. Mestecky, M. W. Russell, S. Jackson, S. M. Michalek, H. Tlaskalová-Hogenová, J. Šterzl) Springer, Boston, MA **1995**, pp. 685–690.
[4] J. Fryer, J. Firca, J. Leventhal, B. Blondin, A. Malcolm, D. Ivancic, R. Gandhi, A. Shah, W. Pao, M. Abecassis, D. Kaufman, F. Stuart, B. Anderson, *Xenotransplantation* **1999**, *6*, 98.
[5] W. E. Walsh, B. E. Anderson, D. Ivancic, Z. Zhang, J. P. Piccini, T. G. Rodgers, W. Pao, J. P. Fryer, *Immunology* **2000**, *101*, 467.
[6] Y. Xu, X. Li, L. Jin, Y. Zhen, Y. Lu, S. Li, J. You, L. Wang, *Biotechnol. Adv.* **2011**, *29*, 860.
[7] U. Gadde, T. Rathinam, H. S. Lillehoj, *Anim. Health Res. Rev.* **2015**, *16*, 163.
[8] M. Mitsunaga, M. Ogawa, N. Kosaka, L. T. Rosenblum, P. L. Choyke, H. Kobayashi, *Nat. Med.* **2011**, *17*, 1685.
[9] K. Sato, T. Nagaya, Y. Nakamura, T. Harada, P. L. Choyke, H. Kobayashi, *Oncotarget* **2015**, *6*, 19747.
[10] K. Sato, N. Sato, B. Xu, Y. Nakamura, T. Nagaya, P. L. Choyke, Y. Hasegawa, H. Kobayashi, *Sci. Transl. Med.* **2016**, *8*, 352ra110.
[11] T. Nagaya, Y. Nakamura, K. Sato, T. Harada, P. L. Choyke, H. Kobayashi, *Mol. Oncol.* **2016**, *10*, 1404.
[12] T. Nakajima, K. Sato, H. Hanaoka, R. Watanabe, T. Harada, P. L. Choyke, H. Kobayashi, *BMC Cancer* **2014**, *14*, 389.
[13] H. Hanaoka, T. Nakajima, K. Sato, R. Watanabe, *Nanomedicine* **2015**, *10*, 1139.
[14] Y. Isobe, K. Sato, Y. Nishinaga, K. Takahashi, S. Taki, H. Yasui, M. Shimizu, R. Endo, C. Koike, N. Kuramoto, H. Yukawa, S. Nakamura, T. Fukui, K. Kawaguchi, T. F. Chen-Yoshikawa, Y. Baba, Y. Hasegawa, *EBioMedicine* **2020**, *52*, 102632.
[15] Y. Nishinaga, K. Sato, H. Yasui, S. Taki, K. Takahashi, M. Shimizu, R. Endo, C. Koike, N. Kuramoto, S. Nakamura, T. Fukui, H. Yukawa, Y. Baba, M. K. Kaneko, T. F. Chen-Yoshikawa, H. Kobayashi, Y. Kato, Y. Hasegawa, *Cells* **2020**, *9*, 1019.
[16] J. J. Zhang, T. Y. Kang, T. Kwon, H. Koh, N. Chandimali, D. L. Huynh, X. Z. Wang, N. Kim, D. K. Jeong, A. A. Han, H. N. Currie, M. S. Loos, G. Scardoni, J. V. Miller, N. Prince, J. A. Mouch, J. W. Boyd, **2019**, 136.
[17] R. Baskaran, J. Lee, S.-G. Yang, *Biomater. Res.* **2018**, *22*, 25.
[18] H. Mahmoudi, A. Bahador, M. Pourhajibagher, M. Y. Alikhani, *J. Lasers Med. Sci.* **2018**, *9*, 154.
[19] G. B. Kharkwal, S. K. Sharma, Y. Y. Huang, T. Dai, M. R. Hamblin, *Lasers Surg. Med.* **2011**, *43*, 755.
[20] Z. Hu, J. Li, H. Liu, L. Liu, L. Jiang, K. Zeng, *Photodiagn. Photodyn. Ther.* **2018**, *23*, 362.
[21] Y. Fu, Y. Bao, Y. Hui, X. Gao, M. Yang, J. Chang, *Photodiagn. Photodyn. Ther.* **2016**, *13*, 29.
[22] X. Lei, B. Liu, Z. Huang, J. Wu, *Arch. Dermatol. Res.* **2015**, *307*, 49.
[23] N. L. Oleinick, H. H. Evans, *Radiat. Res.* **1998**, *150*, S146.
[24] F. Cieplik, D. Deng, W. Crielaard, W. Buchalla, E. Hellwig, A. Al-Ahmad, T. Maisch, *Crit. Rev. Microbiol.* **2018**, *44*, 571.
[25] R. Aminov, *Biochem. Pharmacol.* **2017**, *133*, 4.
[26] Y. Muragaki, J. Akimoto, T. Maruyama, H. Iseki, S. Ikuta, M. Nitta, K. Maebayashi, T. Saito, Y. Okada, S. Kaneko, A. Matsumura, T. Kuroiwa, K. Karasawa, Y. Nakazato, T. Kayama, *J. Neurosurg.* **2013**, *119*, 845.
[27] K. Sato, K. Ando, S. Okuyama, S. Moriguchi, T. Ogura, S. Totoki, H. Hanaoka, T. Nagaya, R. Kokawa, H. Takakura, M. Nishimura, Y. Hasegawa, P. L. Choyke, M. Ogawa, H. Kobayashi, *ACS Cent. Sci.* **2018**, *4*, 1559.
[28] H. Kobayashi, P. L. Choyke, *Acc. Chem. Res.* **2011**, *44*, 83.
[29] K. Sato, R. Watanabe, H. Hanaoka, T. Harada, T. Nakajima, I. Kim, C. H. Paik, P. L. Choyke, H. Kobayashi, *Mol. Oncol.* **2014**, *8*, 620.
[30] K. Sato, T. Nagaya, M. Mitsunaga, P. L. Choyke, H. Kobayashi, *Cancer Lett.* **2015**, *365*, 112.
[31] K. Sato, P. L. Choyke, H. Kobayashi, *PLoS One* **2014**, *9*, e113276.
[32] E. S. Spivak, K. E. Hanson, *J. Clin. Microbiol.* **2018**, *56*, e01588.
[33] A. Bren, Y. Hart, E. Dekel, D. Koster, U. Alon, *BMC Syst. Biol.* **2013**, *7*, 27.
[34] T. Kawamoto, J. D. Sato, A. Le, J. Polikoff, G. H. Sato, J. Mendelsohn, *Proc. Natl. Acad. Sci., U. S. A.* **1983**, *80*, 1337.
[35] G. Monfrecola, E. M. Procaccini, M. Bevilacqua, A. Manco, G. Calabrò, P. Santoianni, *Photochem. Photobiol. Sci.* **2004**, *3*, 419.
[36] H. Kobayashi, P. L. Choyke, *Acc. Chem. Res.* **2019**, *52*, 2332.
[37] Y. Maruoka, T. Nagaya, K. Sato, F. Ogata, S. Okuyama, P. L. Choyke, H. Kobayashi, *Mol. Pharmaceutics* **2018**, *15*, 3634.
[38] S. Okuyama, T. Nagaya, K. Sato, F. Ogata, Y. Maruoka, P. L. Choyke, H. Kobayashi, *Oncotarget* **2018**, *9*, 11159.

[39] K. Nakajima, T. Kimura, H. Takakura, Y. Yoshikawa, A. Kameda, T. Shindo, K. Sato, H. Kobayashi, M. Ogawa, *Oncotarget* **2018**, *9*, 20048.
[40] E. S. M. Ibrahim, A. K. M. S. Rahman, R. Isoda, K. Umeda, N. Van Sa, Y. Kodama, *Vaccine* **2008**, *26*, 2073.
[41] R. E. Faith, L. W. Clem, *Immunology* **1973**, *25*, 151.
[42] U. K. Laemmli, *Nature* **1970**, *227*, 680.
[43] R. Watanabe, K. Sato, H. Hanaoka, T. Harada, T. Nakajima, I. Kim, C. H. Paik, A. M. Wu, P. L. Choyke, H. Kobayashi, *ACS Med. Chem. Lett.* **2014**, *5*, 411.
[44] K. Sato, A. P. Gorka, T. Nagaya, M. S. Michie, R. R. Nani, Y. Nakamura, V. L. Coble, O. V. Vasalatiy, R. E. Swenson, P. L. Choyke, M. J. Schnermann, H. Kobayashi, R. R. Nani, V. L. Coble, O. V. Vasalatiy, R. E. Swenson, P. L. Choyke, M. J. Schnermann, H. Kobayashi, *Bioconjugate Chem.* **2015**, *27*, 404.
[45] A. Chindamporn, Y. Nakagawa, M. Homma, H. Chibana, M. Doi, K. Tanaka, *Microbiology* **1995**, *141*, 469.
[46] K. Morimoto, T. Ozawa, K. Awazu, N. Ito, N. Honda, S. Matsumoto, D. Tsuruta, *PLoS One* **2014**, *9*, e105173.